Title

Flash Formation of I-Rich Clusters during Multistage Halide Segregation Studied in MAPbI1.5Br1.5

Journal

The Journal of Physical Chemistry C, 124(45)

ISSN

1932-7447

Authors

Babbe, Finn

Masquelier, Eloïse

Zheng, Zhi

et al.

Publication Date

2020-11-12

DOI

10.1021/acs.jpcc.0c07063

Peer reviewed

Flash Formation of I-rich Clusters During Multi-Stage Halide Segregation Studied in $MAPbI_{1.5}Br_{1.5}$

Finn Babbe[1]‡, Eloïse Masquelier[1]‡, Zhi Zheng[1,2] and Carolin M. Sutter-Fella[1*]

[1] Chemical Sciences Division, Joint Center for Artificial Photosynthesis, Lawrence Berkeley National Laboratory, Berkeley, USA

[2] Berkeley Extension, University of California Berkeley, Berkeley, USA

* Corresponding author: csutterfella@lbl.gov

Abstract

Wide bandgap mixed halide perovskites such as $MAPb(I_{1-x}Br_x)_3$ sparked great research interest due to their outstanding optoelectronic properties, ease of fabrication and bandgap tunability. Their application thus far is however limited by light-induced halide segregation in which microscopic clusters with high iodide content are formed and act as recombination centers. The key mechanism(s) underlying this halide segregation process are still debated. Here we present a study on the photoluminescence evolution in $MAPb(I_{1.5}Br_{1.5})$ perovskites with varying microstructure under constant illumination at room temperature and at elevated temperature. Our findings reveal a more complicated picture of the segregation mechanism occurring in three stages instead of two as commonly reported. The process starts with a flash formation of I-rich nanodomains. Following is a rapid blue shift before the gradual and typically observed red shift occurs. The evolution of the three stages is fully reversible in the dark and is also present at elevated temperatures (50 °C). We explain the existence of multiple stages during light-induced halide segregation by natural compositional fluctuations of the halides and the formation of halide clusters with a dynamically changing distribution in I-Br content. The variation in I-Br ratio depends on the grain size and film heterogeneity. These findings add further details in the quest of

unraveling the underlying segregation mechanism(s) which need to be identified in order to stabilize halides in wide bandgap perovskites.

Introduction

Hybrid halide perovskites have emerged as promising materials for the next generation of photovoltaic technologies[1] and other optoelectronic applications.[2–7] They have attracted incredible research interest due to their impressive optoelectronic properties such as high absorption coefficient,[8,9] high carrier diffusion length,[10–12] and large defect tolerance.[13,14] In addition, their bandgaps can be tuned almost over the entire visible spectrum via halide substitution. Noh et al. demonstrated that the bandgap of $MAPb(I_{1-x}Br_x)_3$ (methylammonium lead iodide bromide) can be varied via halide alloying from 1.57 eV ($MAPbI_3$) to 2.3 eV ($MAPbBr_3$).[15] The unique properties, as well as ease of inexpensive fabrication make halide perovskites a perfect candidate as wide bandgap top absorber in tandem solar cells. Ideally, the bandgap of the top cell is ~1.7-1.8 eV corresponding to a Br content of ~35 %[15] to maximize performance.[16,17] However, the development for commercial applications has been impeded by the instability of mixed halide perovskite absorbers under illumination. Light induced halide segregation was first observed by photoluminescence (PL) measurements on $MAPb(I_{1-x}Br_x)_3$.[18] The measured PL emission initially corresponds to the well mixed I-Br composition but gradually shifts towards lower emission energies until stabilized at an energy of ~1.68 eV corresponding to ~20 % Br.[18–21] A more complex picture has been recently suggested by Suchan et al., reporting an initial red-shift PL peak (~1.70 eV) in $MAPb(I_{1-x}Br_x)_3$ perovskite films which prominence depends on sample preparation and composition. Based on different PL measurements (spatially resolved and time resolved) they attributed this short-lived peak to small I-rich or pure iodide clusters and suggest that several intermediate stages might take place during halide segregation.[22] X-ray diffraction (XRD) techniques demonstrate the splitting of diffraction peaks under illumination further evidencing photo-induced structural changes.[18,19] This instability has been attributed to the segregation of small parts of the perovskite film into I-rich and Br- rich domains within a predominantly well-mixed phase. Since the I-rich domains have a smaller bandgap than the surrounding material they act as carrier traps and channel free carriers before they recombine radiatively.[18,23] Independent of the initial halide composition, similar iodide contents of about 20 % are found inside

the clusters after segregation.[18] Interestingly, this segregation reverses when the samples are kept in the dark for extended time periods.[18,24,25]

This general phenomenon has been widely reported[18,19,26–28] and has been observed for a wide range of composition.[29–31] However, the underlying mechanism and origin of the phase segregation is still under debate. Multiple theories and mechanisms have been proposed to explain the phenomenon and are discussed in recent review articles by Brennan et al.[29,32] and Knight et al.[30] Overall, three main theories emerged over time. The first one is based on thermodynamics considering differences in free energy to drive the segregation which stem from fluctuations in composition and/or electronic structure.[33–35] The second theory proposes polaronic effects as the origin for halide segregation[36–38] where the lattice strain induced by the electron-phonon coupling yields the formation of I-rich clusters, which number increases over time.[36] The third theory is based on local electric field caused by charge carrier gradients to rationalize the halide segregation.[21,25,34,39] The interaction of the electric fields with charged defects and charge carriers combined with different halide mobilities is argued to drive the observed de-mixing of halides.

In literature the perovskite film crystallinity and morphology are reported to greatly influence halide segregation. Although the detailed mechanisms are still under debate, an improved stability has been observed for films with larger grain sizes and crystallinity.[30,40–43] Obviously, larger grains lead to a strongly reduced amount of grain boundaries in which vicinity often low bandgap domains are detected after illumination.[36,44] Passivation of grain boundaries and interfaces has been reported to slow down segregation[21,41] indicating their importance for the segregation process. It should be noted though that Mao et al. showed that halide segregation also occurs in single crystals suggesting that grain boundaries or associated defects are not an essential requirements for phase segregation.[20] Mixed results regarding the halide mobility at grain boundaries have been reported. On the one hand it has been shown that halide movement is facilitated at grain boundaries.[41,45–47] On the other hand it has been shown that grain boundaries impede ion migration and act as defect trap sites.[48–50]

Also the defect concentration within the perovskite film has also been reported to greatly affect phase segregation, in particular its kinetics.[21,35] By combining theory and experiment a linear dependence between halide vacancy density and halide segregation rate was shown.[35] Overall, reducing the defect density has been proposed to reduce halide segregation.[26,30,35] In

addition, compositional tuning has been reported to mitigate halide segregation mainly via cation substitution.[29,30] Depending on the underlying mechanism assumed, improvements have been linked to stiffening of the crystal structure thus reducing polaronic effects[36,37] but also to general changes in the crystal structure like grain size, grain boundaries, trap state density and halide vacancies.[30] It is thus not straight forward to unravel the relationship of photo stability and compositions, since the latter is highly intertwined with structural factors affecting the halide segregation.

Despite recent efforts no cohesive theory explaining all the findings has emerged so far.[32] However a detailed mechanistic understanding is necessary to overcome or exploit light-driven halide segregation. In our study we investigate the influence of microstructure, namely the grain size and film heterogeneity, on the initial halide segregation process of $MAPb(I_{0.5}Br_{0.5})_3$ films to gain insights into the driving mechanism. Measurements carried out at room temperature and at 50 °C suggest that halide segregation occurs via 3 stages, independently of the grain size, heterogeneity and temperature. This differs from the commonly reported 2 stages observed by PL measurements in which besides the mixed phase a low energy peak appears that then continuously red shifts over time. We find an intermediate stage in which the PL corresponding to the iodide rich phase shows a blue shift for a couple of seconds. We link this shift to the initial flash formation of I-rich nanodomains with very low iodide content. Over time additional clusters with higher bromide content form leading to a blue shift in the conjunct PL peak position. The composition of those clusters is dynamically changing over time and depend on the average grain size and film heterogeneity. These results give more insights to the underlying segregation mechanism which is needed to develop a detailed mechanistic understanding of the process and to stabilize wide bandgap perovskites.

Experimental Section

Film Fabrication: Perovskite precursor solutions were prepared in nitrogen atmosphere by dissolving MAI (Greatcell, > 99%), MABr (Sigma Aldrich, 98%), PbI_2 (TCI, 99.99%) and $PbBr_2$ (TCI) in equimolar ratios in dimethylformamide (DMF) (Sigma Aldrich, anhydrous, 99.8 %). All chemicals were used as received. Glass substrates (1.2 x 1.2 cm) where cleaned as described by Saliba et al.[51] $MAPb(I_{0.5},Br_{0.5})_3$ films were prepared in a solvent engineering process via spin coating. First, 50 µL precursor solution are deposited on the substrate and dispersed in a slow step (5 s at 1000 rpm)

followed by a fast step (35 s at 5000 rpm). Second, 200 µL of the anti-solvent chlorobenzene (CB) are rapidly dropped at various times after initial spin coated started (9 s and 13 s). After spin coating the samples are annealed on a hot plate at 100 °C for various times (30 s / 2 min / 10 min). To protect samples from oxidation and changes during measurements all samples are covered with poly(methyl methacrylate) (PMMA) layer. For this 5 mg of PMMA (Tokyo Chemical Industry Co.) is dissolved in 1 mL chlorobenzene (CB, from Sigma Aldrich, 99.8 %) by stirring the solution at 70°C for 12 hours. Then, the solution is spin casted on the annealed samples.

Characterization: To quantify morphology and grain size distribution scanning electron images (SEM) images are taken using a FEI Quanta FEG 250 with acceleration voltage of 5 kV. The grain size was determined by manually redrawing grain boundaries, determining the crystal area, and calculating the diameter assuming a round shape. X-ray diffraction (XRD) spectra are recorded to verify the composition and check for possible secondary phases using a Rigaku SmartLab. Photoluminescence measurements are carried out in a home-built set-up using a 532 nm laser excitation (Obis LX, 0.1 mm diameter). Emitted photons are collected by a 50x objective and focused into an optical fiber for detection in a grating monochromator (Ocean Optics, QE Pro). Reflected laser light is filtered by a long pass filter (Thorlabs, HLP550) in the collimated beam. If not stated otherwise a peak power density of 15 mW/cm^2 was used during the measurements corresponding to 0.5 equivalent suns. To evaluate the number of suns, the number of photons absorbed by the perovskite layer (with fixed bandgap of 1.88 eV) under AM1.5 illumination is determined and compared to the number of photons emitted from the monochromatic excitation source. PL spectra are background corrected, transformed into energy space and fitted using two gaussian profiles (Supporting Information Figure S1).

Results

$MAPb(I_{0.5}Br_{0.5})_3$ thin films are prepared with different grain sizes and various degrees of homogeneity by varying the annealing time or antisolvent dropping time, respectively (see experimental section and SI for details). Representative SEM top view images together with grain size histograms are shown in Figure 1a-d) and in the Supporting Information Figure S2. Heterogeneous samples exhibit a wide grain size distribution from a few tens of nm up to 1 µm (Figure 1c,d). X-ray diffraction (XRD) patterns (Figures 1c,f,

S3a) confirm phase purity. The XRD full width at half maximum (FWHM) is decreasing for longer annealing times as reflected by an increasing grain size observed by SEM (Supporting Information Figure S2). The heterogeneous film however, displays a higher XRD peak intensity, originating from the stronger scattering of large domains, and a broader FWHM (Figure 1e,f).

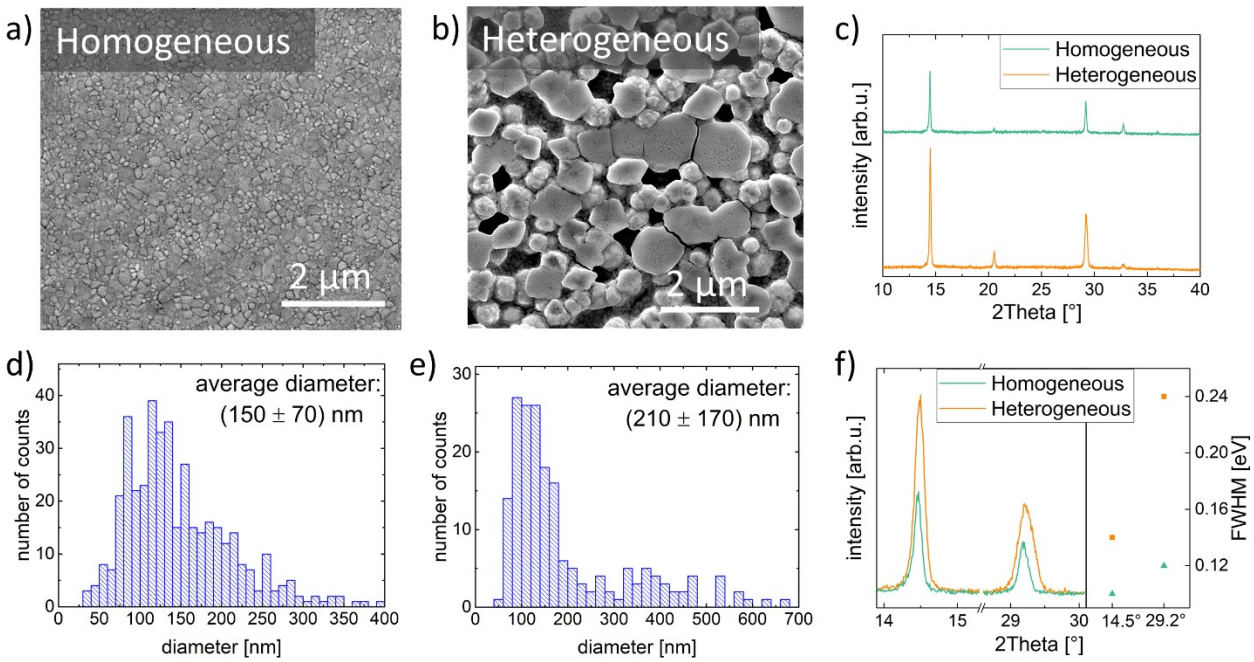

Figure 1. SEM images of the prepared $MAPb(I_{0.5}Br_{0.5})_3$ perovskite films. Shown are a homogeneous sample with ~150 nm grain size (a) and a heterogeneous sample (b) as well as their respective grain size distributions (d,e). c) X-ray diffraction patterns of both samples as well as f) zoomed diffraction patterns and FWHM of the dominant peaks.

In order to study halide segregation, photoluminescence (PL) spectra are continuously measured over the course of 15 minutes at room temperature and fixed illumination density (λ = 532 nm, ~0.5 equivalent suns). To visualize the dynamics of halide segregation, Figure 2 displays normalized contour plots of the homogeneous and heterogeneous sample together with a selection of time dependent spectra measured on the heterogeneous sample for the first 30 seconds. Initially, a peak at ~1.88 eV is observed matching the bandgap of a mixed perovskite with 50 % bromide (marked as stage I in Figures 2a,b).[19,34] A few seconds later a second peak at lower energies emerges which intensity increases over time (stage II). The low

energy peak is short lived and gradually shifts towards higher energies accompanied by a significant peak broadening. In stage III, PL emission gradually red shifts and increases further in intensity. Since the exact energetic positions vary with respect to microstructure as well as from sample to sample we decided to describe observed trends qualitatively. Thus far, the so-called Hoke-effect, refers to a process that initially showed PL emission at high energy corresponding to the well mixed perovskite phase (same as above described stage I) followed by emission at ~1.7 eV that exhibits a continuous and gradual red shift corresponding to luminescence of an I-rich phase (same as above described stage III) where charge carriers are funneled to recombination due to its lower bandgap.[18]

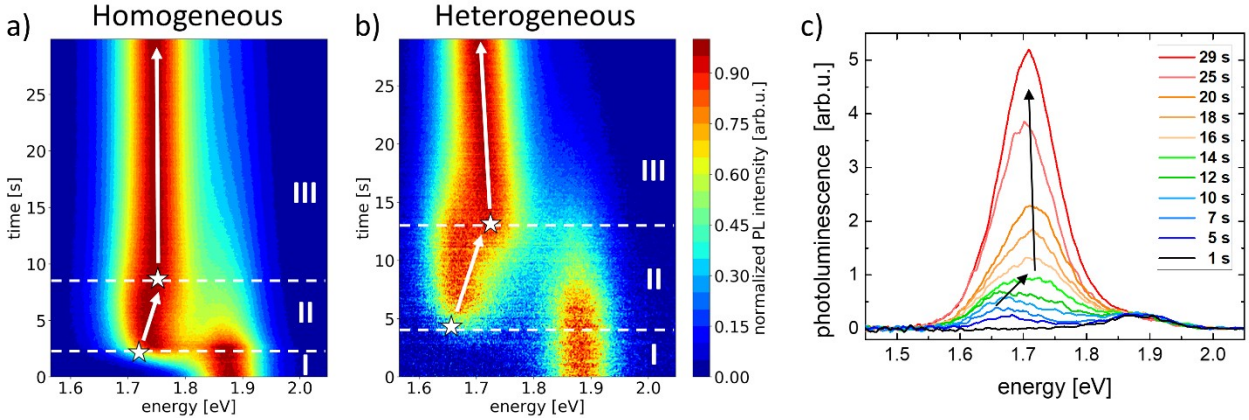

Figure 2. a) Contour plots of normalized PL spectra showing the first 30 s of the halide segregation process for a homogeneous film (a) and a heterogeneous film (b). The stars indicate the peak position of the low energy PL emission and the arrows represent a guide to the eye on how this peak shifts over time. c) Selected PL spectra of a heterogeneous film during segregation. The arrow shows the time evolution of a total of 25 s.

Unlike in previous studies[18,19,29,34] we found a blue shift of the PL emission as described for stage II in this work. Given the short-lived nature of the initial low energy emission at the transition between stage I and II we will refer to it as flash formation of I-rich clusters. This back and forth shift (rapid blue shift followed by a gradual red shift) is most obvious in the heterogeneous sample (Figure 2b) but appears in all samples measured, as shown in Figures 2a) and Supporting Information Figure S4. The magnitude and kinetics of the shift however, strongly depend on the microstructure. For an in-depth

analysis, the PL spectra are fitted with two gaussians tracking the evolution of the high and low energy PL peaks over time (more details on the fitting routine are described in the SI). Figure 3a) illustrates the key parameters extracted from the data fitting for the I-rich PL (low energy) peak. E_0 describes the initial low energy PL peak position related to the flash formation of I-rich clusters and E_f the final peak position after 15 minutes of continuous illumination. ΔE defines the magnitude of the blue shift in stage II. The extracted parameters can be correlated to the average grain size as shown in Figure 3b) depicting average values from multiple data sets. The individual data sets are shown in the Supporting Information Figure S6. Looking at the initial peak position (E_0) a clear trend with grain size is observed where E_0 is the increases steadily with increasing grain size. The same increasing trend is observed for the final peak position. The magnitude of the blue shift (ΔE) decreases with grain size from ~40 meV to ~20 meV. Looking at the heterogeneous sample an intermediate blue shift is determined but lower E_0 and E_f values compared to the homogenous samples.

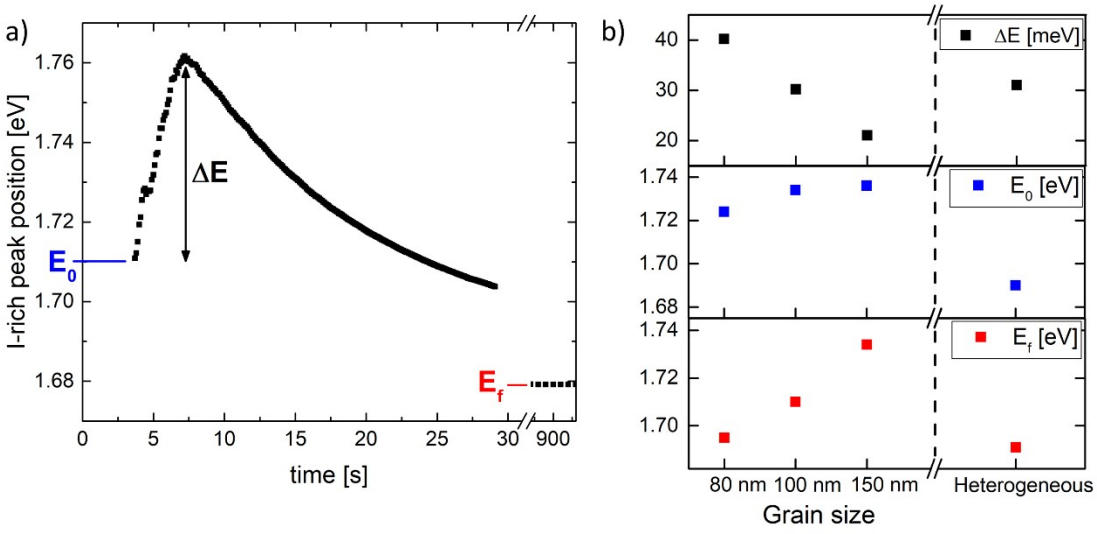

Figure 3. a) Evolution of the peak position of the I-rich PL peak together with the key features namely initial energy (E_0), magnitude of the blueshift (ΔE), and final peak position (E_f). b) Comparison of those key features for perovskites films with varying average grain size as well as heterogeneous microstructure.

In addition, the PL FWHM and intensity of the emission corresponding to the iodide rich phase are plotted for different microstructures (Supporting Information Figure S5). In all cases the intensity gradually increases over time in agreement with previous reports.[18,25] Looking at the FWHM for all samples an initially narrow peak (110-120 meV) is observed which broadens during stage II before it narrows again and continues to narrow in stage III. Comparing multiple sets of various grain size and morphology a good reproducibility of the above described trends is found (Supporting Information Figure S6).

Next, we repeated the PL measurements at 50°C and made similar observations as described above. The three stages of halide segregation seen at room temperature also occur at elevated sample temperatures at least for small grain or heterogeneous samples but with faster kinetics (Supporting Information Figure S7). Since the emergence of the low energy peak occurs at an earlier time and the blue shift happens faster no clear shifts could be identified for samples with large grains. The amplitude of ΔE is a bit smaller but similar to the one at room temperature indicating that the temperature affects mainly the kinetics but not the mechanism of the halide segregation. This assumption is supported by XRD measurements after the PL measurements showing no change in the crystal structure and no peak related to PbI_2 which would indicate an irreversible decomposition of the absorber layer (Supporting Information Figure S3b). This also rules out a loss of iodide from the composition which has been previously reported to cause a blue shift to be the origin of stage II.[52,53] The faster kinetics observed at 50 °C are in agreement to literature reports showing that the rate of halide segregation follows an Arrhenius behavior with an activation energy close to one for halide migration.[18,27,34]

The phenomenon of halide segregation (or Hoke effect) is known to be reversible which means if samples are kept in the dark for prolonged time PL emission will again show up at high energies representing the sample in its mixed halide distribution state.[25] To verify reversibility of the complex halide segregation proceeding in three stages, samples are kept in the dark for ~30 minutes followed by consecutive PL measurements. The flash formation of very I-rich clusters followed by a rapid blue shift (stage II) is consistently observed during several cycles of dark recovery and illumination (Supporting Information Figure S8a). The same key parameters of the I-rich phase (E_0, E_f, ΔE) are found for each cycle varying only by a few meV (Supporting Information Figure S8b).

Discussion

All samples investigated showed three stages of halide segregation. In stage I high energy emission of the well mixed I-Br clusters is observed (Figure 4a). In stage II a second peak appears at low energy representative of very I-rich clusters gradually blue shifting (compare schematic Figure 4). Finally, in stage III a steady red shift of the low energy peak is observed. This finding adds a new stage to the previously reported Hoke effect where halide segregation proceeds in two steps, basically as described here for the stages I and III. Stage II that includes the flash formation of very I-rich clusters confirms the recent observation reported by Suchan et al regarding the existence of a temporary low energy PL peak.[22] They reported the existence of a temporary low-energy PL peak (~1.70 eV) in $MAPb(I_{1-x}Br_x)_3$ perovskite films which prominence depends on sample preparation and composition.[22] Based on different PL measurements (spatially resolved and time resolved) they attributed this short-lived peak to small I-rich or pure iodide clusters and suggest that several intermediate stages might take place during halide segregation.[22] Our major focus of this study is to understand how the microstructure of $MAPb(I_{0.5}Br_{0.5})_3$ affects the halide segregation. Thus, PL response of thin films with different grain sizes and varying levels of heterogeneities were compared. The discussion of trends following below is qualitative due to variations from sample to sample caused by inadvertent deviations in the synthesis or sample handling. The described trends however, were found to be fairly robust and were measured in multiple sample sets at room temperature (Supporting Information Figure S6) as well as 50 °C, and are fully reversible in dark/illumination cycles (Supporting Information Figure S8).

Comparing different grain sizes, a steady increase of the initial (E_0) and final (E_f) peak position of the iodide rich luminescence is found with increasing grain size (Figure 3b). This trend indicates higher halide (iodide) mobility in films with small grains. Generally, in polycrystalline films there are two mechanisms for ion migration, either through defects in the bulk or along grain boundaries. Smaller grains mean a higher grain boundary density which is correlated to a considerable defect density found at grain boundaries. The role of the GBs is under discussion in literature with evidence for completely opposite trends showing either enhanced halide migration[45,47] or indications for inhibited GB movement of halides.[48–50] We attribute the linear increase in E_0 and E_f with grain size to an enhanced halide migration along the grain boundaries. ΔE which can be regarded as a

measure for the spread in compositional cluster distribution confirms this interpretation.

A second plausible explanation for the trend observed with grain size originates in the high density of strain related neutral defects in the vicinity of grain boundaries. This explanation would follow the interpretation by Knight et al. who identified those defects to act as carrier traps under illumination, thus causing local electric fields driving the segregation.[54] Samples with higher grain boundary density have a higher density of those defects, making the formation of very I-rich cluster more likely thus, explaining the lower E_0 and the larger ΔE.

Comparing different levels of heterogeneities, it is found that the most heterogeneous sample with large grain size distribution ranging from many grains with diameter ~50-100 nm to 1 µm shows the smallest E_0 as well as E_f. This observation cannot be explained by the trend with grain size observed and the grain boundary density alone but indicates other effective driving forces that facilitate halide movement in films with heterogeneous microstructure such as lattice strain and halide defects.[21,36,54] Given that heterogeneous samples were fabricated by applying a non-ideal antisolvent drop time we assume that this condition induces a high defect density in the bulk of individual grains facilitating halide segregation via both, grain boundary and intra grain diffusion. ΔE of the heterogeneous sample does not show a similar extreme as E_0 and E_f suggesting competing halide diffusion mechanisms in films with heterogeneous microstructure.

Overall, we explain the apparent existence of multiple stages during light induced halide segregation by the formation of halide clusters with a distribution in I-Br content. This is proposed to depend on grain size as well as microstructural heterogeneity and is illustrated in the qualitative schematic Figure 4. This schematic shows the evolution of PL emission for small and large grains during stages I and II. From the measured PL we estimated Br content and number of clusters , roughly taking charge funneling into low bandgap regions[18,55] as well as variation in PL quantum yield with Br composition[56] into consideration. It is noted that PL measurements provide a distribution of emitting states and that it cannot be used to obtain a quantitative amount of I-Br cluster distribution since a multitude of factors like charge carrier diffusion, lifetime, funneling, and a compositional variation of the PL quantum yield influence the luminescence.[18,55,56] This leads to the fact the PL is most sensitive to radiative emission from the lowest energy transition. Therefore, the initial flash formation of I-

rich clusters in stage II (Figure 4b) indicates the presence of a small amount of clusters with very low Br content which are likely co-present with other compositional halide clusters and which are more pronounced in thin films with small grains facilitated by halide migration along grain boundaries.

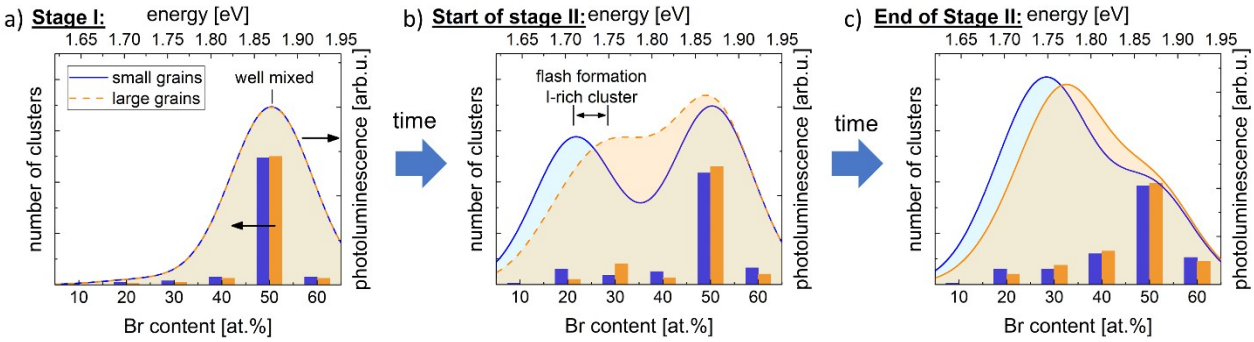

Figure 4. Proposed qualitative model for the multi-stage halide segregation. The line plots (solid/dashed) depict the observed PL emission within the experiment for a small grain sample (blue) and a large grain sample (orange). The bar plot describes the estimated number of clusters with a certain Br content leading to the measured PL spectrum. In the beginning of stage 2 (b) a small number of clusters with very low bromide content (< 25 %) channel the radiative recombination leading to the emergence of a low energy PL peak. In the following more clusters with low bromide form (25 % < x < 50 %) leading to a broadening of the low energy peak towards higher energies. Over time those clusters with higher Br content dominate the low energy peak causing the conjunct peak to blue shift in stage II.

Underlying our interpretation are natural compositional fluctuations of the halides that are present even in pristine samples in the dark as argued by Limmer et al.[37] Similarly, Knight et al. described random thermal movements of halides and free carriers to cause I-rich regions.[25] These fluctuations can lead to charge carrier trapping causing local electric fields.[25,28] The presence of an electric field in the film increases the extent of halide segregation and consequently further drives charge separation leading to a stronger electric field. This cycle happening under illumination can not only be used to explain co-existence of clusters with different halide ratios but also their change over time as the strength of the electric field changes. Consequently, we explain the observed blue shift in stage II by the super position of PL coming from I-rich clusters with various halide ratios (Figure 4 b,c). Initially only PL from clusters with the lowest bromide content is observed due to the charge

carrier funneling into those clusters (Figure 4b). Further PL from the well mixed phase is observed, since only part of the generated carriers reach those global bandgap minima due to limited charge carrier lifetime and carrier mobility as well as possible trap states.

However, over time I-rich clusters with higher bromide ratio form as more and more defects trap carriers and cause local electric fields. The amount of those clusters increases over time, since the probability to form is higher compared to the nearly iodide pure nanodomains (which mostly formed already). At some point, those higher bandgap I-rich clusters outnumber the low bandgap clusters and thus also appear in the PL spectra at a slightly higher emission energy since they act as local bandgap minima channeling recombination (Figure 4c). While the PL from the nanodomains stays constant, the PL intensity of this second peak increases over time as the number of clusters grows. The small difference of the respective peak positions causes a great overlap between both spectra making them almost indistinguishable and leading to a somewhat asymmetric peak shape. The intensity of the second peak increases over time, causing the joint low energy peak to broaden and blue shift as observed in stage II. At the end of stage II (Figure 4c), the PL intensity from the initially formed I-rich clusters has diminished to a remaining low energy shoulder. A more detailed overview how the different compositions contribute to the measured PL over the cause of the segregation process is shown in Supporting Information Figure S9.

Our interpretation is supported by narrowband PL imaging measurements on single crystal $MAPb(Br_xI_{1-x})_3$ performed by Mao et al.[20] They found a complex sequence of rapidly changing emission spectra. Over the course of a few tens of seconds not only emission intensity but also emission energy is changing and in particular, multiple emission energies are found to co-exist at a given time. Besides the decay of the mixed phase, they observe the appearance of a monotonically red shifting second peak and a growing broad peak centered ~720 nm (1.72 eV) corresponding to highly I-rich nanodomains.[20] Over time the PL of the nanodomains hardly changes whereas the I-rich clusters continuously shifts towards lower energies. Although in our measurements, the I-rich nanodomains appear first, possibly due to the different diffusion mechanisms in polycrystalline thin films versus single crystals, a comparison between our findings and the report by Mao et al.[20] provides clear evidence for multiple complex stages occurring during halide segregation.

Conclusions

In this study we intentionally manipulate the microstructure of $MAPb(I_{0.5}Br_{0.5})_3$ thin films to investigate light induced halide segregation with respect to grain size and film inhomogeneity that is, wide grain size distribution between tens of nm up to µm. Our PL results experimentally indicate that halide segregation occurs via three distinct and robust stages independent of microstructure, which are reversible after storage in the dark and visible at room temperature as well as at 50 °C.

We interpret the overall trends by the co-existence of I-Br clusters with varying halide ratio in accordance with previous experimental reports on $MAPb(I_{1-x}Br_x)_3$ single crystals.[20] This halide ratio is dynamically changing over time and the underlying cause for the observed stages. The PL signal is most sensitive to low Br-containing clusters due to carrier funneling leading to an initial PL emission at energies close to pure $MAPbI_3$ at the beginning of stage II. Over time I-rich clusters with higher Br form and become active sites for a significant amount of radiative recombination leading to a gradual blue shift PL in stage II. Stage III follows the in literature reported red shift with a concurrent increase in intensity.

We found a linear increase of E_0 with grain size indicating that grain boundaries play a role in the halide segregation process. We propose that a faster halide mobility along the grain boundaries assists the formation of the initial I-rich nanodomains. The reported trends correlate with grain size and are reproducible for different sample sets, but exact numbers differ slightly. We link this to minor differences in the synthesis conditions which lead to variations in the natural compositional fluctuations of the halides, as argued by Limmer et al.[37]

In conclusion, our study reveals the existence of three stages instead of the previously reported two stages during halide segregation upon illumination. We propose a spread of clusters with varying halide ratio which are dynamically changing to be the cause for the complex shifting process of the I-rich PL emission. The stages exist for different microstructures, as well as at elevated temperatures and are reversible when stored in the dark. Given the robust trend we believe that these findings may apply to other previous halide segregation investigations. Our study adds another piece to the puzzle of understanding the proceeding stages during halide segregation.

Associated Content

Supporting Information:

Detailed description of precursor preparation, substrate cleaning, film deposition and annealing processes. PL measurement protocol and exemplary fit curves. Additional SEM, XRD and PL data for the investigated sample series. Statistical overview of PL results from other sample sets. PL measurement data from a reversibility study as well as from measurements at elevated temperature.

Author Information

Corresponding Author

*Carolin M. Sutter-Fella - Chemical Sciences Division, Joint Center for Artificial Photosynthesis, Lawrence Berkeley National Laboratory, Berkeley, USA – ORCID: 0000-0002-7769-0869

Authors

‡ Finn Babbe - Chemical Science Division, Joint Center for Artificial Photosynthesis, Lawrence Berkeley National Laboratory, Berkeley, USA – ORCID: 0000-0002-9131-638X

‡ Eloïse Masquelier - Chemical Science Division, Joint Center for Artificial Photosynthesis, Lawrence Berkeley National Laboratory, Berkeley, USA

Zhi Zheng – i) Chemical Science Division, Joint Center for Artificial Photosynthesis, Lawrence Berkeley National Laboratory, Berkeley, USA ii) Berkeley Extension, University of California Berkeley, Berkeley, USA

Author contribution

‡ F.B. and E.M. contributed equally to manuscript. C.M.S.-F. initiated and directed this research. E.M. and Z.Z. prepared samples and analyzed them by SEM and XRD. F.B. and E.M. conducted PL experiments and evaluated the data. F.B., E.M. and C.M.S.-F. wrote the manuscript. All authors commented on the manuscript and given approval to the final version.

Notes

The authors declare no competing financial interest.

Acknowledgements

This material is based upon work performed by the Joint Center for Artificial Photosynthesis, a DOE Energy Innovation Hub, supported through the Office of Science of the U.S. Department of Energy under Award Number DE-SC0004993.

References

(1) National Renewable Energy Laboratory. *Best Research-Cell Efficiencies*; 2020.

(2) Hou, Y.; Aydin, E.; De Bastiani, M.; Xiao, C.; Isikgor, F. H.; Xue, D.-J.; Chen, B.; Chen, H.; Bahrami, B.; Chowdhury, A. H. et al. Efficient Tandem Solar Cells with Solution-Processed Perovskite on Textured Crystalline Silicon. *Science* **2020**, *367* (6482), 1135–1140. https://doi.org/10.1126/science.aaz3691.

(3) Huang, H.; Pradhan, B.; Hofkens, J.; Roeffaers, M. B. J.; Steele, J. A. Solar-Driven Metal Halide Perovskite Photocatalysis: Design, Stability, and Performance. *ACS Energy Lett.* **2020**, *5* (4), 1107–1123. https://doi.org/10.1021/acsenergylett.0c00058.

(4) Quan, L. N.; García de Arquer, F. P.; Sabatini, R. P.; Sargent, E. H. Perovskites for Light Emission. *Advanced Materials* **2018**, *30* (45), 1801996. https://doi.org/10.1002/adma.201801996.

(5) Lin, K.; Xing, J.; Quan, L. N.; de Arquer, F. P. G.; Gong, X.; Lu, J.; Xie, L.; Zhao, W.; Zhang, D.; Yan, C.; et al. Perovskite Light-Emitting Diodes with External Quantum Efficiency Exceeding 20 per Cent. *Nature* **2018**, *562* (7726), 245–248. https://doi.org/10.1038/s41586-018-0575-3.

(6) Wei, H.; Fang, Y.; Mulligan, P.; Chuirazzi, W.; Fang, H.-H.; Wang, C.; Ecker, B. R.; Gao, Y.; Loi, M. A.; Cao, L.; Huang, J. Sensitive X-Ray Detectors Made of Methylammonium Lead Tribromide Perovskite Single Crystals. *Nature Photon* **2016**, *10* (5), 333–339. https://doi.org/10.1038/nphoton.2016.41.

(7) Xing, G.; Mathews, N.; Lim, S. S.; Yantara, N.; Liu, X.; Sabba, D.; Grätzel, M.; Mhaisalkar, S.; Sum, T. C. Low-Temperature Solution-Processed Wavelength-Tunable Perovskites for Lasing. *Nature Mater* **2014**, *13* (5), 476–480. https://doi.org/10.1038/nmat3911.

(8) Shirayama, M.; Kadowaki, H.; Miyadera, T.; Sugita, T.; Tamakoshi, M.; Kato, M.; Fujiseki, T.; Murata, D.; Hara, S.; Murakami, T. N.; et al. Optical Transitions in Hybrid Perovskite Solar Cells: Ellipsometry, Density Functional Theory, and Quantum Efficiency Analyses for CH3NH3PbI3. *Physical Review Applied* **2016**, *5* (1), 014012. https://doi.org/10.1103/PhysRevApplied.5.014012.

(9) Yin, W.-J.; Shi, T.; Yan, Y. Unique Properties of Halide Perovskites as Possible Origins of the Superior Solar Cell Performance. *Adv. Mater.* **2014**, *26* (27), 4653–4658. https://doi.org/10.1002/adma.201306281.
(10) Stranks, S. D.; Eperon, G. E.; Grancini, G.; Menelaou, C.; Alcocer, M. J. P.; Leijtens, T.; Herz, L. M.; Petrozza, A.; Snaith, H. J. Electron-Hole Diffusion Lengths Exceeding 1 Micrometer in an Organometal Trihalide Perovskite Absorber. *Science* **2013**, *342* (6156), 341–344. https://doi.org/10.1126/science.1243982.
(11) deQuilettes, D. W.; Koch, S.; Burke, S.; Paranji, R. K.; Shropshire, A. J.; Ziffer, M. E.; Ginger, D. S. Photoluminescence Lifetimes Exceeding 8 Ms and Quantum Yields Exceeding 30% in Hybrid Perovskite Thin Films by Ligand Passivation. *ACS Energy Lett.* **2016**, *1* (2), 438–444. https://doi.org/10.1021/acsenergylett.6b00236.
(12) Brenner, T. M.; Egger, D. A.; Kronik, L.; Hodes, G.; Cahen, D. Hybrid Organic—Inorganic Perovskites: Low-Cost Semiconductors with Intriguing Charge-Transport Properties. *Nature Reviews Materials* **2016**, *1* (1), 15007. https://doi.org/10.1038/natrevmats.2015.7.
(13) Steirer, K. X.; Schulz, P.; Teeter, G.; Stevanovic, V.; Yang, M.; Zhu, K.; Berry, J. J. Defect Tolerance in Methylammonium Lead Triiodide Perovskite. *ACS Energy Lett.* **2016**, *1* (2), 360–366. https://doi.org/10.1021/acsenergylett.6b00196.
(14) Ball, J. M.; Petrozza, A. Defects in Perovskite-Halides and Their Effects in Solar Cells. *Nat Energy* **2016**, *1* (11), 16149. https://doi.org/10.1038/nenergy.2016.149.
(15) Noh, J. H.; Im, S. H.; Heo, J. H.; Mandal, T. N.; Seok, S. I. Chemical Management for Colorful, Efficient, and Stable Inorganic-Organic Hybrid Nanostructured Solar Cells. *Nano Lett.* **2013**, *13* (4), 1764–1769. https://doi.org/10.1021/nl400349b.
(16) Kim, D.; Jung, H. J.; Park, I. J.; Larson, B. W.; Dunfield, S. P.; Xiao, C.; Kim, J.; Tong, J.; Boonmongkolras, P.; Ji, S. G.; et al. Efficient, Stable Silicon Tandem Cells Enabled by Anion-Engineered Wide-Bandgap Perovskites. *Science* **2020**, *368* (6487), 155–160. https://doi.org/10.1126/science.aba3433.
(17) Todorov, T.; Gunawan, O.; Guha, S. A Road towards 25% Efficiency and beyond: Perovskite Tandem Solar Cells. *Mol. Syst. Des. Eng.* **2016**, *1* (4), 370–376. https://doi.org/10.1039/C6ME00041J.
(18) Hoke, E. T.; Slotcavage, D. J.; Dohner, E. R.; Bowring, A. R.; Karunadasa, H. I.; McGehee, M. D. Reversible Photo-Induced Trap Formation in Mixed-Halide Hybrid Perovskites for Photovoltaics. *Chem. Sci.* **2014**, *6* (1), 613–617. https://doi.org/10.1039/C4SC03141E.
(19) Brennan, M. C.; Draguta, S.; Kamat, P. V.; Kuno, M. Light-Induced Anion Phase Segregation in Mixed Halide Perovskites. *ACS Energy Letters* **2018**, *3* (1), 204–213. https://doi.org/10.1021/acsenergylett.7b01151.
(20) Mao, W.; Hall, C. R.; Chesman, A. S. R.; Forsyth, C.; Cheng, Y.-B.; Duffy, N. W.; Smith, T. A.; Bach, U. Visualizing Phase Segregation in Mixed-Halide Perovskite Single Crystals. *Angewandte Chemie International*

Edition **2019**, *58* (9), 2893–2898. https://doi.org/10.1002/anie.201810193.
(21) Barker, A. J.; Sadhanala, A.; Deschler, F.; Gandini, M.; Senanayak, S. P.; Pearce, P. M.; Mosconi, E.; Pearson, A. J.; Wu, Y.; Srimath Kandada, A. R.; et al. Defect-Assisted Photoinduced Halide Segregation in Mixed-Halide Perovskite Thin Films. *ACS Energy Lett.* **2017**, *2* (6), 1416–1424. https://doi.org/10.1021/acsenergylett.7b00282.
(22) Suchan, K.; Merdasa, A.; Rehermann, C.; Unger, E. L.; Scheblykin, I. G. Complex Evolution of Photoluminescence during Phase Segregation of MAPb(I1-XBrx)3 Mixed Halide Perovskite. *Journal of Luminescence* **2020**, *221*, 117073. https://doi.org/10.1016/j.jlumin.2020.117073.
(23) Yang, X.; Yan, X.; Wang, W.; Zhu, X.; Li, H.; Ma, W.; Sheng, C. Light Induced Metastable Modification of Optical Properties in CH3NH3PbI3−xBrx Perovskite Films: Two-Step Mechanism. *Organic Electronics* **2016**, *34*, 79–83. https://doi.org/10.1016/j.orgel.2016.04.020.
(24) Yoon, S. J.; Kuno, M.; Kamat, P. V. *Shift Happens* . How Halide Ion Defects Influence Photoinduced Segregation in Mixed Halide Perovskites. *ACS Energy Letters* **2017**, *2* (7), 1507–1514. https://doi.org/10.1021/acsenergylett.7b00357.
(25) Knight, A. J.; Wright, A. D.; Patel, J. B.; McMeekin, D. P.; Snaith, H. J.; Johnston, M. B.; Herz, L. M. Electronic Traps and Phase Segregation in Lead Mixed-Halide Perovskite. *ACS Energy Lett.* **2019**, *4* (1), 75–84. https://doi.org/10.1021/acsenergylett.8b02002.
(26) Slotcavage, D. J.; Karunadasa, H. I.; McGehee, M. D. Light-Induced Phase Segregation in Halide-Perovskite Absorbers. *ACS Energy Lett.* **2016**, *1* (6), 1199–1205. https://doi.org/10.1021/acsenergylett.6b00495.
(27) DeQuilettes, D. W.; Zhang, W.; Burlakov, V. M.; Graham, D. J.; Leijtens, T.; Osherov, A.; Bulović, V.; Snaith, H. J.; Ginger, D. S.; Stranks, S. D. Photo-Induced Halide Redistribution in Organic-Inorganic Perovskite Films. *Nature Communications* **2016**, *7* (May). https://doi.org/10.1038/ncomms11683.
(28) Yoon, S. J.; Draguta, S.; Manser, J. S.; Sharia, O.; Schneider, W. F.; Kuno, M.; Kamat, P. V. Tracking Iodide and Bromide Ion Segregation in Mixed Halide Lead Perovskites during Photoirradiation. *ACS Energy Letters* **2016**, *1* (1), 290–296. https://doi.org/10.1021/acsenergylett.6b00158.
(29) Brennan, M. C.; Ruth, A.; Kamat, P. V.; Kuno, M. Photoinduced Anion Segregation in Mixed Halide Perovskites. *Trends in Chemistry* **2020**, *2* (4), 282–301. https://doi.org/10.1016/j.trechm.2020.01.010.
(30) Knight, A. J.; Herz, L. M. Preventing Phase Segregation in Mixed-Halide Perovskites: A Perspective. *Energy Environ. Sci.* **2020**, 10.1039.D0EE00788A. https://doi.org/10.1039/D0EE00788A.
(31) Beal, R. E.; Hagström, N. Z.; Barrier, J.; Gold-Parker, A.; Prasanna, R.; Bush, K. A.; Passarello, D.; Schelhas, L. T.; Brüning, K.; et al. Structural Origins of Light-Induced Phase Segregation in Organic-Inorganic Halide

Perovskite Photovoltaic Materials. *Matter* **2020**, *2* (1), 207–219. https://doi.org/10.1016/j.matt.2019.11.001.
(32) Kuno, M.; Brennan, M. C. What Exactly Causes Light-Induced Halide Segregation in Mixed-Halide Perovskites? *Matter* **2020**, *2* (1), 21–23. https://doi.org/10.1016/j.matt.2019.12.004.
(33) Brivio, F.; Caetano, C.; Walsh, A. Thermodynamic Origin of Photoinstability in the CH3NH3Pb(I1–XBrx)3 Hybrid Halide Perovskite Alloy. *J. Phys. Chem. Lett.* **2016**, *7* (6), 1083–1087. https://doi.org/10.1021/acs.jpclett.6b00226.
(34) Draguta, S.; Sharia, O.; Yoon, S. J.; Brennan, M. C.; Morozov, Y. V.; Manser, J. S.; Kamat, P. V.; Schneider, W. F.; Kuno, M. Rationalizing the Light-Induced Phase Separation of Mixed Halide Organic–Inorganic Perovskites. *Nat Commun* **2017**, *8* (1), 1–8. https://doi.org/10.1038/s41467-017-00284-2.
(35) Ruth, A.; Brennan, M. C.; Draguta, S.; Morozov, Y. V.; Zhukovskyi, M.; Janko, B.; Zapol, P.; Kuno, M. Vacancy-Mediated Anion Photosegregation Kinetics in Mixed Halide Hybrid Perovskites: Coupled Kinetic Monte Carlo and Optical Measurements. *ACS Energy Letters* **2018**, *3* (10), 2321–2328. https://doi.org/10.1021/acsenergylett.8b01369.
(36) Bischak, C. G.; Hetherington, C. L.; Wu, H.; Aloni, S.; Ogletree, D. F.; Limmer, D. T.; Ginsberg, N. S. Origin of Reversible Photoinduced Phase Separation in Hybrid Perovskites. *Nano Letters* **2017**, *17* (2), 1028–1033. https://doi.org/10.1021/acs.nanolett.6b04453.
(37) Limmer, D. T.; Ginsberg, N. S. Photoinduced Phase Separation in the Lead Halides Is a Polaronic Effect. *arXiv:2001.01677 [cond-mat, physics:physics]* **2020**.
(38) Wang, X.; Ling, Y.; Lian, X.; Xin, Y.; Dhungana, K. B.; Perez-Orive, F.; Knox, J.; Chen, Z.; Zhou, Y.; Beery, D.; et al. Suppressed Phase Separation of Mixed-Halide Perovskites Confined in Endotaxial Matrices. *Nat Commun* **2019**, *10* (1), 695. https://doi.org/10.1038/s41467-019-08610-6.
(39) Belisle, R. A.; Bush, K. A.; Bertoluzzi, L.; Gold-Parker, A.; Toney, M. F.; McGehee, M. D. Impact of Surfaces on Photoinduced Halide Segregation in Mixed-Halide Perovskites. *ACS Energy Lett.* **2018**, *3* (11), 2694–2700. https://doi.org/10.1021/acsenergylett.8b01562.
(40) Hu, M.; Bi, C.; Yuan, Y.; Bai, Y.; Huang, J. Stabilized Wide Bandgap MAPbBrxI3–x Perovskite by Enhanced Grain Size and Improved Crystallinity. *Adv Sci (Weinh)* **2015**, *3* (6). https://doi.org/10.1002/advs.201500301.
(41) Zhou, Y.; Jia, Y.-H.; Fang, H.-H.; Loi, M. A.; Xie, F.-Y.; Gong, L.; Qin, M.-C.; Lu, X.-H.; Wong, C.-P.; Zhao, N. Composition-Tuned Wide Bandgap Perovskites: From Grain Engineering to Stability and Performance Improvement. *Advanced Functional Materials* **2018**, *28* (35), 1803130. https://doi.org/10.1002/adfm.201803130.
(42) Beal, R. E.; Slotcavage, D. J.; Leijtens, T.; Bowring, A. R.; Belisle, R. A.; Nguyen, W. H.; Burkhard, G. F.; Hoke, E. T.; McGehee, M. D. Cesium

Lead Halide Perovskites with Improved Stability for Tandem Solar Cells. *J. Phys. Chem. Lett.* **2016**, *7* (5), 746–751. https://doi.org/10.1021/acs.jpclett.6b00002.
(43) Braly, I. L.; Stoddard, R. J.; Rajagopal, A.; Uhl, A. R.; Katahara, J. K.; Jen, A. K.-Y.; Hillhouse, H. W. Current-Induced Phase Segregation in Mixed Halide Hybrid Perovskites and Its Impact on Two-Terminal Tandem Solar Cell Design. *ACS Energy Letters* **2017**, *2* (8), 1841–1847. https://doi.org/10.1021/acsenergylett.7b00525.
(44) Tang, X.; Van Den Berg, M.; Gu, E.; Horneber, A.; Matt, G. J.; Osvet, A.; Meixner, A. J.; Zhang, D.; Brabec, C. J. Local Observation of Phase Segregation in Mixed-Halide Perovskite. *Nano Letters* **2018**, *18* (3), 2172–2178. https://doi.org/10.1021/acs.nanolett.8b00505.
(45) Shao, Y.; Fang, Y.; Li, T.; Wang, Q.; Dong, Q.; Deng, Y.; Yuan, Y.; Wei, H.; Wang, M.; Gruverman, A.; Shield, J.; Huang, J. Grain Boundary Dominated Ion Migration in Polycrystalline Organic–Inorganic Halide Perovskite Films. *Energy & Environmental Science* **2016**, *9* (5), 1752–1759. https://doi.org/10.1039/C6EE00413J.
(46) Yuan, Y.; Huang, J. Ion Migration in Organometal Trihalide Perovskite and Its Impact on Photovoltaic Efficiency and Stability. *Acc. Chem. Res.* **2016**, *49* (2), 286–293. https://doi.org/10.1021/acs.accounts.5b00420.
(47) Yun, J. S.; Seidel, J.; Kim, J.; Soufiani, A. M.; Huang, S.; Lau, J.; Jeon, N. J.; Seok, S. I.; Green, M. A.; Ho-Baillie, A. Critical Role of Grain Boundaries for Ion Migration in Formamidinium and Methylammonium Lead Halide Perovskite Solar Cells. *Adv. Energy Mater.* **2016**, *6* (13), 1600330. https://doi.org/10.1002/aenm.201600330.
(48) Phung, N.; Al-Ashouri, A.; Meloni, S.; Mattoni, A.; Albrecht, S.; Unger, E. L.; Merdasa, A.; Abate, A. The Role of Grain Boundaries on Ionic Defect Migration in Metal Halide Perovskites. *Adv. Energy Mater.* **2020**, *10* (20), 1903735. https://doi.org/10.1002/aenm.201903735.
(49) Correa-Baena, J.-P.; Anaya, M.; Lozano, G.; Tress, W.; Domanski, K.; Saliba, M.; Matsui, T.; Jacobsson, T. J.; Calvo, M. E.; Abate, A.; et al. Unbroken Perovskite: Interplay of Morphology, Electro-Optical Properties, and Ionic Movement. *Adv. Mater.* **2016**, *28* (25), 5031–5037. https://doi.org/10.1002/adma.201600624.
(50) Nie, W.; Tsai, H.; Asadpour, R.; Blancon, J.-C.; Neukirch, A. J.; Gupta, G.; Crochet, J. J.; Chhowalla, M.; Tretiak, S.; Alam, M. A.; et al. High-Efficiency Solution-Processed Perovskite Solar Cells with Millimeter-Scale Grains. *Science* **2015**, *347* (6221), 522–525. https://doi.org/10.1126/science.aaa0472.
(51) Saliba, M.; Correa-Baena, J.-P.; Wolff, C. M.; Stolterfoht, M.; Phung, N.; Albrecht, S.; Neher, D.; Abate, A. How to Make over 20% Efficient Perovskite Solar Cells in Regular (n–i–p) and Inverted (p–i–n) Architectures. *Chemistry of Materials* **2018**, *30* (13), 4193–4201. https://doi.org/10.1021/acs.chemmater.8b00136.
(52) Li, Y.; Xu, X.; Wang, C.; Ecker, B.; Yang, J.; Huang, J.; Gao, Y. Light-Induced Degradation of $CH_3NH_3PbI_3$ Hybrid Perovskite Thin Film. *J.*

Phys. Chem. C **2017**, *121* (7), 3904–3910. https://doi.org/10.1021/acs.jpcc.6b11853.
(53) Zhang, H.; Fu, X.; Tang, Y.; Wang, H.; Zhang, C.; Yu, W. W.; Wang, X.; Zhang, Y.; Xiao, M. Phase Segregation Due to Ion Migration in All-Inorganic Mixed-Halide Perovskite Nanocrystals. *Nat Commun* **2019**, *10* (1), 1088. https://doi.org/10.1038/s41467-019-09047-7.
(54) Knight, A. J.; Patel, J. B.; Snaith, H. J.; Johnston, M. B.; Herz, L. M. Trap States, Electric Fields, and Phase Segregation in Mixed-Halide Perovskite Photovoltaic Devices. *Adv. Energy Mater.* **2020**, *10* (9), 1903488. https://doi.org/10.1002/aenm.201903488.
(55) Andaji-Garmaroudi, Z.; Abdi-Jalebi, M.; Guo, D.; Macpherson, S.; Sadhanala, A.; Tennyson, E. M.; Ruggeri, E.; Anaya, M.; Galkowski, K.; Shivanna, R.; et al. A Highly Emissive Surface Layer in Mixed-Halide Multication Perovskites. *Adv. Mater.* **2019**, *31* (42), 1902374. https://doi.org/10.1002/adma.201902374.
(56) Sutter-Fella, C. M.; Li, Y.; Amani, M.; Ager, J. W.; Toma, F. M.; Yablonovitch, E.; Sharp, I. D.; Javey, A. High Photoluminescence Quantum Yield in Band Gap Tunable Bromide Containing Mixed Halide Perovskites. *Nano Letters* **2016**, *16* (1), 800–806. https://doi.org/10.1021/acs.nanolett.5b04884.

TOC image